Physicochem. Probl. Miner. Process., 61(4), 2025, 206993 | Physicochemical Problems of Mineral Processing

http://www.journalssystem.com/ppmp | ISSN 1643-1049

Equal-thickness screening mechanism of multi-mass vibrating flip-flow screens

Sanpeng Gong [1,2], Fuqiang Zhang [1], Ningning Xu [1,2], Guofeng Zhao [1,2], Bowei Liu [1], Jialiang Guo [1], Yifan Guo [1]

[1] School of Mechanical and Power Engineering, Henan Polytechnic University, Jiaozuo 454003, China

[2] Henan Province Engineering Technology Research Center for Coal Mine Mechanical Equipment, Jiaozuo, 454003, China

Corresponding author: 18813089516@163.com (Sanpeng Gong)

Abstract: The vibrating flip-flow screen (VFFS) is extensively employed for screening moist fine-grained minerals. However, prevalent uniform-amplitude VFFSs often suffer from material accumulation and suboptimal screening efficiency. In this paper, a dynamic model of the multi-mass VFFS was established using the multi-mass dynamics theory, and the amplitude regulation in different regions of the multi-mass VFFS was achieved by adjusting the mass of the floating screen frame (FSF), thereby revealing the regulation mechanism of the variable-amplitude VFFS. Leveraging the coupling advantages of the finite element method (FEM) and discrete element method (DEM), a simulation model of the interaction between multiple flip-flow screen panels and minerals was constructed. The kinematic characteristics of particles and the screen panel under constant and variable amplitude conditions for the VFFS were analyzed, respectively, and the impact of dynamic parameters on screening performance was investigated. A three-factor and three-level orthogonal experimental design, combined with response surface optimization, was used to assess the influence of screen panel inclination, angular frequency, and relative amplitudes of the main screen frame (MSF) and FSF on the screening performance and time. The results indicated that the optimal solutions considering both screening efficiency and screening time can be achieved when the relative amplitude of the three regions of variable-amplitude VFFS are 4 mm, 6 mm, and 8 mm, respectively, the screen inclination was 11°, and the angular frequency was 76 $rad \cdot s^{-1}$.

Keywords: multi-mass dynamics, variable-amplitude, equal-thickness screening, vibrating flip-flow screen, FEM-DEM co-simulation

1. Introduction

The dry deep screening of moist fine-grained minerals is a difficult problem that urgently needs to be solved in the current mineral processing industry (Shi et al., 2025). When using conventional vibrating screens with rigid screen panels to screen moist fine-grained minerals, screen panel blinding and aperture plugging occur, leading to poor screening efficiency (Hou et al., 2024; Xu et al., 2024). The vibrating flip-flow screen (VFFS), by taking advantage of the large-deflection bending deformation generated by its elastic screen panel during the reciprocating motion, can effectively address problems like screen panel aperture blocking and sticking during the screening of moist fine-grained coal (Wu et al., 2025). However, the amplitude of each part of the screen panel of the dual-mass VFFS is consistent during its operation, resulting in the problems of mineral accumulation at the feed end and low utilization rate of the screen panel (Li et al., 2021; Lin et al., 2023). Therefore, exploring the dynamic characteristics of the variable-amplitude VFFS and the mechanism of equal-thickness screening is of great significance for improving the screening performance of the VFFS, and the research in this regard has attracted extensive attention.

Xiong et al. (2017) established the linear dynamic model and the vibration differential equation of the conventional VFFS using the two-degree-of-freedom vibration theory, and expressions for the

DOI: 10.37190/ppmp/206993

displacement amplitudes of the main screening frame (MSF) and the floating screening frame (FSF) under the steady state are derived, revealing the reasonable operation area of the VFFS through the amplitude-frequency characteristic curve. Gong et al. (2019; 2020) proposed a nonlinear dynamic model for the VFFS by integrating a novel dynamic model of shear spring that precisely captures the amplitude and frequency-dependent behaviour of shear springs, and experimental validations were conducted to demonstrate the rationality of the proposed VFFS dynamic model. Lin et al. (2022; 2023) considered the impact of screen panel tension on the dynamics of the VFFS system, proposed a dynamic model of VFFS taking the dynamics of the screen panel into account, and the influence of related parameters on the system's dynamics are analyzed. Wu et al. (2020) took the influence of the material on the screen panel into account and established a dynamic model of the crank-link type flip-flow screen system using the lumped mass method. Through dynamic theoretical analysis, the correlation between the material mass and the motion parameters is deduced. Yu et al. (2021) analysed the vibration stability of the VFFS under different operation conditions and investigated its screening performance under various scenarios. They demonstrated that the material load on the screen panel would affect the vibration stability of VFFS, and the reasonable operational area of the VFFS is in the near anti-resonance region. However, these researches mainly focused on the dynamics of conventional equal-amplitude VFFS, and the dynamics of variable-amplitude VFFS and its variable-amplitude regulation mechanism were not deeply investigated.

Screening minerals with adjusting amplitude or inclination angle of the screen panel can effectively prevent the accumulation of minerals, achieving approximately equal-thickness screening of the minerals on the screen panel, and thus improving the screening performance (Jiang et al. 2017; Duan et al. 2021). Dong et al. (2009) conducted a numerical simulation to investigate the physical separation curves and the distribution of minerals passing through the screen panel of the equal-thickness screening under the conditions of three-section and five-section segmented screen panels. It is found that the accumulation of minerals is determined by the movement of the minerals on the screen panel. An appropriate movement speed can increase the screening rate, while a relatively low mineral speed is likely to cause the accumulation of materials. Fernandez et al. (2011) employed a coupled discrete element method-smoothed particle hydrodynamics (DEM-SPH) model to investigate the screening process of moist particles using a double-layer equal-thickness vibrating screen and determined the effects of bed thickness and density on particle flow patterns. Jiang et al. (2024) adopted the theory of an equal-thickness screen in the combined vibrating screen, thereby realizing its operation at variable frequencies. A new concept of combined excitation parameters was proposed, offering supplementary adjustable factors for the vibrating screen. This innovation significantly enhanced the efficiency of achieving a consistent thickness of the material layer on the screening panel, optimizing the screening performance. Qiao et al. (2018) considered the material velocity, the change in layer thickness, and the distribution characteristics of particle groups on the screen panel, comparatively analysed the movement laws of the overall feed particle group under constant-amplitude and variable-amplitude conditions, and investigated the influence of different factors on the screening performance of the variable- amplitude equal-thickness vibrating screen. Huang et al. (2022) established a mechanical model for the collision between particles and a multistage variable-inclination screening panel. It was found that the maximum collision force is closely related to the amplitude, frequency, inclination angle of the screening surface, and the number of screening panel stages. Moreover, the penetration screening laws of particle groups on the screening panel were revealed. These studies primarily focus on the regulatory mechanisms governing variable-amplitude equal-thickness screening for the vibrating screens with rigid screen panels, yet they lack investigations into the equal-thickness screening mechanisms for the VFFS.

The kinematic characteristics of particle collisions on the flip-flow screen panel directly determine the processing capacity and screening performance of the VFFS. Akbari et al. (2017) analysed the screening performance of a flip-flow screen during 1 mm and 2 mm classification, demonstrating that separation efficiency is higher when the particle size range of coal samples is narrow and decreases as the particle size range widens. The flip-flow screens exhibit superior screening performance when classifying wet fine-grained materials was revealed, providing critical insights into their application for challenging screening tasks involving moisture-laden particles. Wang et al. (2024) utilized a coupled multi-body dynamics and discrete element method (MFBD-DEM) to simulate the flip-flow screening process. The simulation results were validated via analysis of variance (ANOVA), and subsequent optimization of vibration parameters was conducted to enhance screening performance. Wu et al (2019) and Zhang et al. (2019) approximated the flip-flow screen panel as a flexible structure based on catenary theory and conducted a co-simulation of the bidirectional coupling between mineral particles and the screen panel using EDEM and RecurDyn software. This study analysed the influence laws of eccentric mass, screen panel inclination, and feed particle size composition on screening efficiency, productivity, and particle motion velocity, providing theoretical insights into parameter optimization for flip-flow screens. Zhao et al. (2023) integrated the advantages of the finite element method (FEM) and discrete element method (DEM) to propose a coupled FEM-DEM simulation approach capable of characterizing the dynamic behaviour of flip-flow screen panels and minerals under heavy-load conditions. The kinematic characteristics of mixed particles on the screen panel were revealed, offering a deeper understanding of the loosening and stratification mechanisms of mineral aggregates during screening. Therefore, the above research illustrates that the FEM-DEM coupling method can be used to simulate the dynamic interaction between the flip-flow screen panel and minerals, thereby investigating the equal-thickness screening process of variable amplitude VFFS.

This paper applies the multi-mass dynamics theory to develop the dynamic model of the investigated multi-mass VFFS, and its variable amplitude regulation mechanism was revealed. A simulation model of the coupling system encompassing multiple screen panels and mineral particles is constructed using the FEM-DEM coupling method, and the kinematic characteristics of particles and the screen panel under constant and variable amplitude conditions for the VFFS were analyzed, respectively. Subsequently, a three-factor and three-level orthogonal experimental design, integrated with response surface optimization, was employed to evaluate the impact of the screen panel inclination, the angular frequency, and the relative amplitudes of MSF and FSF on the screening performance and the screening time, and the optimal solution that can simultaneously consider both the screening performance and the screening time are obtained.

2. Dynamic analysis of multi-mass VFFS

The VFFS is composed of the main screen frame (MSF) and the floating screen frame (FSF). The MSF vibrates under the action of exciting force. Through the action of the shear springs, the MSF is also induced to vibrate. When a specific exciting frequency is reached, the screen panel installed on MSF

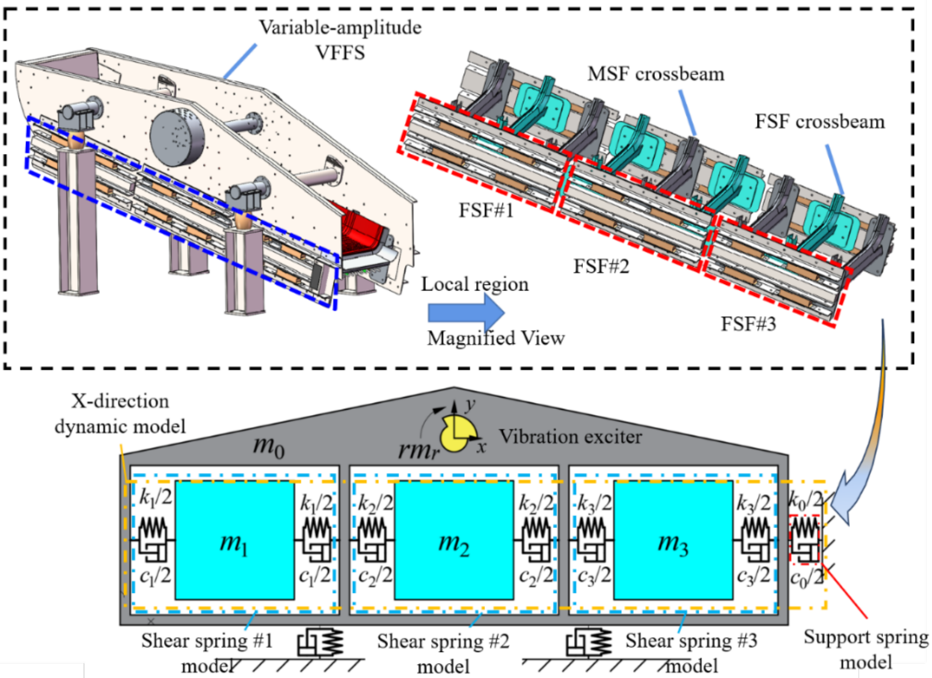

Fig. 1. Dynamic model of multi-mass VFFS

and the FSF generate relative motion. This leads to the tension and relaxation of the screen panel, thereby achieving the screening of wet fine-grained minerals. Conventional constant-amplitude VFFS, which maintain uniform vibration amplitudes across the entire screening zone, often encounter challenges such as mineral accumulation and low screening efficiency. To address these limitations, based on the multi-mass vibration theory, the FSF is partitioned into three sections, and variable amplitude in different regions can be achieved by adjusting the dynamic parameters of the vibration system, as illustrated in Fig. 1, where, m_0 represents the mass of the MFS, while m_1, m_2, and m_3 denote the masses of FSMs 1, 2, and 3, respectively. The stiffness and damping coefficient of the isolation springs are designated as k_0 and c_0, respectively. Correspondingly, k_1, k_2, and k_3 represent the stiffness of shear springs 1, 2, and 3, with c_1, c_2, and c_3 indicating their respective damping coefficients. The parameter rm_r is the mass moment of the exciter eccentric block. Since the screen panel of VFFS mainly performs tension and relaxation motion in the x-direction, this paper ignores the influence in the y-direction, because the MSF and FSF will vibrate synchronously in the y-direction when VFFS works, which causes little effect on the performance of the VFFS. Therefore, in this paper, the dynamics of the multi-mass VFFS were studied only considering x-direction (Gong et al. 2018). When the exciter applies a harmonic excitation force $\boldsymbol{F}_{\text{exit}}=rm_{\text{r}}\omega^2\cos(\omega t)$ to the MSF of VFFS, according to the multi-mass dynamics theory, the differential equations for the motion of the multi-mass VFFS are established as follows (Guo et al., 2024):

$$\begin{cases} m_0\ddot{x}_0 = F_{\text{exit}} - c_0\dot{x}_0 + \sum_{i=1}^{4} c_i(\dot{x}_i - \dot{x}_0) - k_0x_0 + \sum_{i=1}^{4} k_i(x_i - x_0) \\ m_1\ddot{x}_1 = c_1(\dot{x}_0 - \dot{x}_1) + k_1(x_0 - x_1) \\ m_2\ddot{x}_2 = c_2(\dot{x}_0 - \dot{x}_2) + k_2(x_0 - x_2) \\ m_3\ddot{x}_3 = c_3(\dot{x}_0 - \dot{x}_3) + k_3(x_0 - x_3) \end{cases} \tag{1}$$

To simplify the analysis, let $F_{\text{in}}=-rm_r\cos(\omega t)$, thus $F_{\text{exit}}=\ddot{F}_{\text{in}}$ .Then, the system of differential Eq. 1 can be written in matrix form:

$$\mathbf{M}\ddot{\mathbf{X}} + \mathbf{C}\dot{\mathbf{X}} + \mathbf{K}\mathbf{X} = \mathbf{F} \tag{2}$$

In Eq. 2, X= $[x_0, x_1, x_2, x_3]^{\text{T}}$ and F= $[\ddot{F}_{\text{in}}, 0, 0, 0]^{\text{T}}$ denote the displacement and excitation force vector of the VFFS system. The matrices M, C, and K represent the mass, damping, and stiffness matrix of the system, with their explicit formulations provided as follows:

$$\mathbf{M} = \begin{pmatrix} m_0 & & & \\ & m_1 & & \\ & & m_2 & \\ & & & m_3 \end{pmatrix}, \quad \mathbf{C} = \begin{pmatrix} \sum_{i=0}^{3} c_i & -c_1 & -c_2 & -c_3 \\ -c_1 & c_1 & & \\ -c_2 & & c_2 & \\ -c_3 & & & c_3 \end{pmatrix}, \quad K = \begin{pmatrix} \sum_{i=0}^{3} k_i & -k_1 & -k_2 & -k_3 \\ -k_1 & k_1 & & \\ -k_2 & & k_2 & \\ -k_3 & & & k_3 \end{pmatrix}$$

Applying the Laplace transform to both sides of Eq. 2, with s denoting the Laplace transform variable, yields the dynamic stiffness matrix:

$$\begin{cases} Z(s)X(s) = F(s) \\ Z(s) = M + \dfrac{C}{s} + \dfrac{K}{s^2} \end{cases} \tag{3}$$

Then, the transfer function matrix $\boldsymbol{G}(s)$ can be written as:

$$G(s) = Z(s)^{-1} \tag{4}$$

In $\boldsymbol{G}(s)$, the elements of the first column are the transfer functions of the MSF and the three FSMs. Then, the steady-state responses of the MSF and FSMs are derived as:

$$\begin{cases} x_0(t) = rm_{\text{r}}\left|g_0(j\omega)\right|\cos[\omega t + (\angle g_0(j\omega) + \pi)] \\ x_i(t) = rm_{\text{r}}\left|g_i(j\omega)\right|\cos[\omega t + (\angle g_i(j\omega) + \pi)] \end{cases} \tag{5}$$

In Eq. 5, j^2=-1, $|g_0(j\omega)|$ and $\angle g_0(j\omega)$ represents the amplitude and phase angle of the MSF, while $|g_i(j\omega)|$ and $\angle g_i(j\omega)$ corresponds to the amplitude and phase angle of the i^{th} FSM.

Based on Eq. 5, the amplitude-frequency response and phase-frequency response of the MSF and FSF can be expressed as (Guo et al. 2024):

$$\begin{cases} A_i(\omega) = rm_r |g_i(j\omega)| \\ \varphi_i(\omega) = -[\angle g_i(j\omega) + \pi] \end{cases} \tag{6}$$

Based on the dynamic response of the FFS2461-type dual-mass VFFS, this study decomposes the FSM of this dual-mass VFFS into three independent floating screen frames, thereby transforming the traditional dual-mass VFFS into a multi-mass VFFS. The parameters of the multi-mass VFFS investigated in this paper, referenced from the FFS2461-type VFFS, are listed in Table 1.

Table 1. Parameters of the multi-mass VFFS

Symbol	Definition	Unit	Value
m_0	Mass of the MSF	kg	916
m_i	Mass of the individual FSF	kg	103.3
k_0	Stiffness of the support spring	N/m	602×10^3
ξ_0	Damping ratio of the support spring	/	0.21
k_i	Stiffness of the individual shear spring	N/m	9×10^6
ξ_i	Damping ratio of the individual shear spring	/	0.045
m_r	Mass moment of the vibrator's eccentric block	kg.m	3.69

To investigate the dynamic response of the multi-mass VFFS, the mass of FSF 1 was reduced by 20%, the mass of FSF 2 was kept constant, and the mass of FSF 3 was increased by 20%. The resulting dynamic response of the multi-mass VFFS is illustrated in Fig. 2.

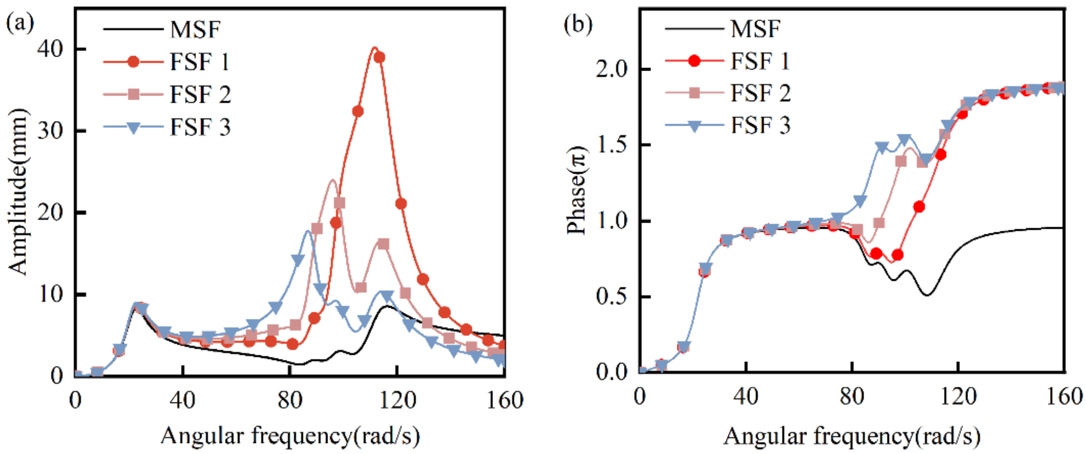

Fig. 2. Dynamic response of the investigated multi-mass VFFS: (a) amplitude-frequency response, (b) phase-frequency response

As can be seen from Fig. 2, by adjusting the mass of each FSF in the multi-mass VFFS, variable amplitudes of different FSFs can be achieved, thereby enabling variable amplitude regulation of the screen panel in different regions of the multi-mass VFFS. As indicated by Eq. 6, the displacements of the MSF and FSF can be adjusted by modifying parameters such as shear spring stiffness and the mass of floating frames. By applying an optimization algorithm to regulate these parameters, the relative displacement amplitude between the MSF and FSF can reach a predefined target value, thereby optimizing the screening performance of the multi-mass VFFS. The optimization function is expressed as follows, and the specific optimization process has been discussed by us in Eq. 7:

$$(A_1\ A_2\ \cdots\ A_i)^T = \underset{\substack{\alpha\in R^n \\ \omega=[\omega_{\min},\omega_{\max}]}}{Optimize}\left\{\Gamma(\alpha_1\ \alpha_2\ \cdots\ \alpha_n)^T\right\} \tag{7}$$

3. Establishment of the simulation model of the investigated VFFS

3.1. FEM-DEM model coupling

The discrete element method (DEM) enables the acquisition of microscale particle information that is difficult to measure directly. By solving force and motion equations, DEM can accurately calculate interparticle contacts and the motion states of numerous particles under given conditions, thereby effectively simulating the swarm behaviour of minerals during the screening process. However, DEM has limitations in simulating the motion of flexible bodies, whereas the finite element method (FEM) excels in modelling the deformation and motion of flexible structures. To achieve a more accurate simulation of the VFFS's screening process, this study combines the respective advantages of FEM and DEM to realize a precise description of the screen panel's large deflection bending and dynamic coupling between particles and the screen panel, as shown in Fig. 3.

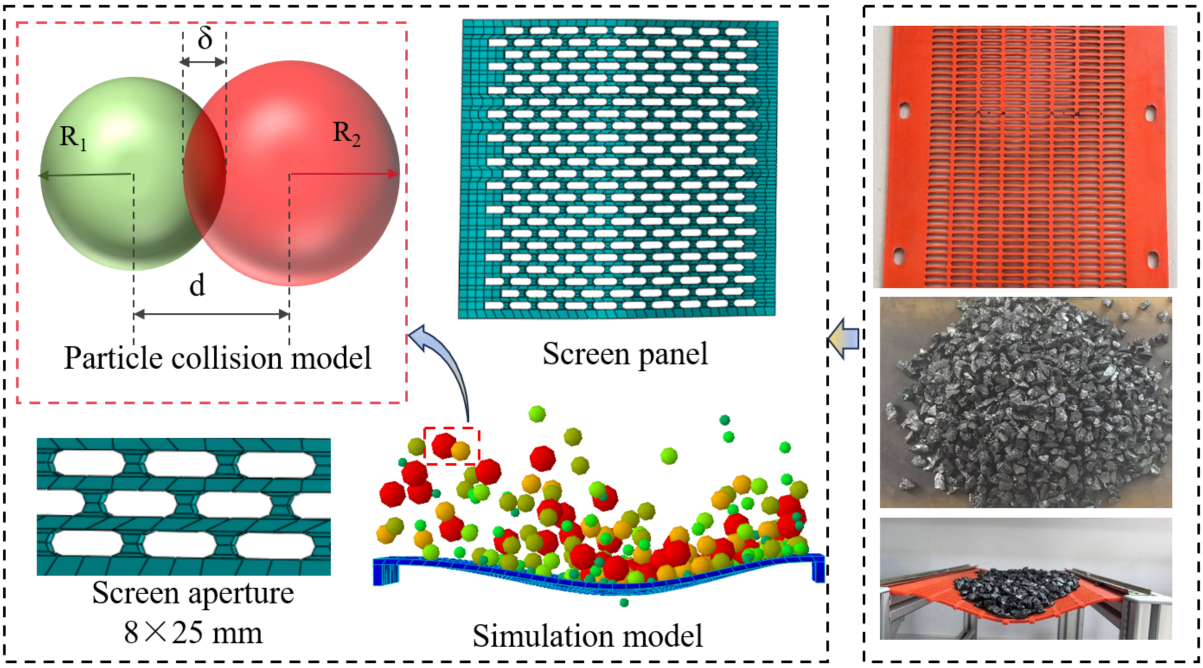

Fig. 3. Schematic diagram of FEM-DEM coupling model

Based on the particle collision model, when the screen panel is loaded with particles, the dynamic parameters such as displacement and velocity between particles under operation conditions can be investigated. According to Newton's second law, the equation of motion governing inter-particle interactions can be described as (Zhao et al., 2010):

$$\begin{cases} m_i \dfrac{\mathrm{d}v_i}{\mathrm{d}t} = \sum\limits_j (F_{ij}^n + F_{ij}^s) + m_i g \\ I_i \dfrac{\mathrm{d}\omega_i}{\mathrm{d}t} = \sum\limits_j (T_{ij}^n + T_{ij}^s) \end{cases} \tag{8}$$

where, m and I denote the mass and moment of inertia of the spherical particle, respectively; v represents the translational velocity; j denotes the total number of particle contacts; F_{ij}^n and T_{ij}^n denote the normal force and normal torque, respectively; F_{ij}^s and T_{ij}^s denote the tangential force and tangential torque, respectively.

According to Hertz's contact theory, the normal contact force between particles is described by a spring-damper model, while the tangential contact force is modelled using a spring-damper-slider model. In this study, the soft-sphere model is employed to calculate particle collision processes (Zheng et al., 2017):

$$\begin{cases} \delta = R_1 + R_2 - \mathrm{d} \\ T_n = 4\boldsymbol{E}^* \sqrt{R}\boldsymbol{\delta}^{\frac{3}{2}} / 3 \\ \dfrac{1}{E^*} = \dfrac{1-\nu_1^{\ 2}}{E_1} + \dfrac{1-\nu_2^{\ 2}}{E_2} \\ R = \dfrac{R_1 R_2}{R_1 + R_2} \end{cases} \tag{9}$$

where T_n denotes the stiffness of the Hertz contact model; R_1 and R_2 denote the radii of the two contacting particles, respectively; d represents the distance between the centers of the two spheres; δ denotes the overlap depth of the two spheres; and E_1, ν_1, E_2, and ν_2 denote the elastic moduli and Poisson's ratios of different particle pairs, respectively.

3.2. The simulation model of the screening process of VFFS

Abaqus software supports a variety of constitutive models, excels in simulating granular material behaviour, and features the capability to define rubber constitutive models. Therefore, the simulation model was constructed in Solidworks software and subsequently imported into Abaqus for finite element analysis. The flip-flow screen panel, made of hyper elastic polyurethane rubber, was described using the Mooney-Rivlin model in the software. Harmonic forces $f(x)=A\sin(\omega t)$ with opposite directions were applied to both ends of the screen panel to achieve alternating tension and relaxation effects. Through the explicit dynamic analysis and particle generation technology of Abaqus, particles are generated above the screen panel by coding in the Abaqus output Inp file, achieving the coupling of finite element and discrete element techniques, as presented in Fig. 4.

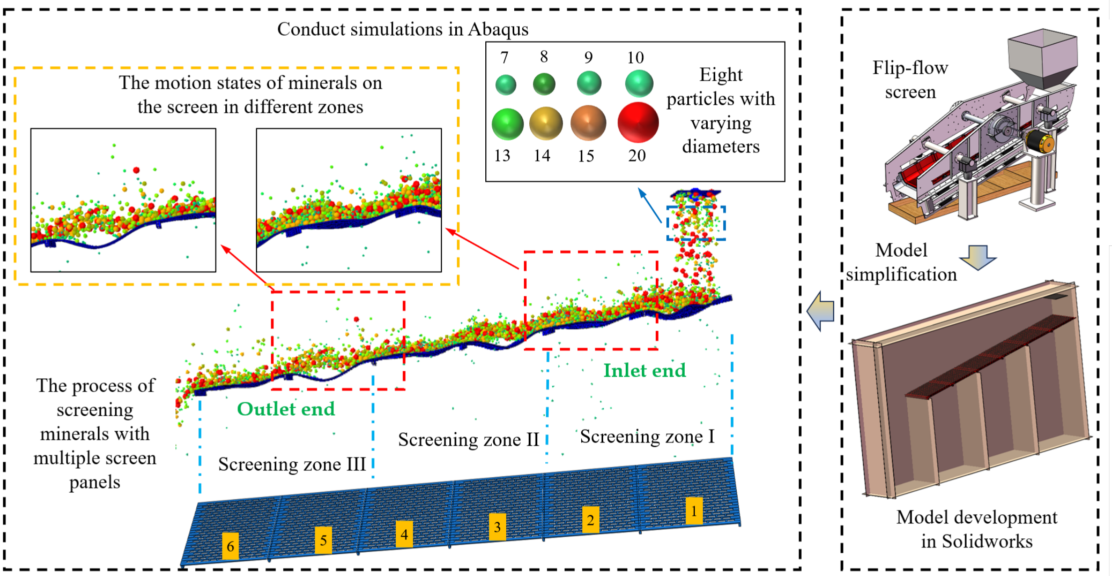

Fig. 4. Establishment of the simulation model of the multi-mass VFFS

In this study, to simulate the mineral accumulation effect at the inlet end while considering the computational duration, the screen inclination angle was configured as 10°-15°, the relative amplitude between the MSF and FSF in different regions was set as 4-8 mm, and the number of screen panels was arranged as 6, with every two screen panels forming a screening zone, resulting in a total of three screening zones. In addition, the selected screen panel has dimensions of 300 mm×328 mm, the screen aperture size is 8 mm×25 mm, and the screen panel thickness is 4 mm, to better simulate the thickness variation of minerals on the screen panel and save simulation time, the width of the screening area is adjusted to 150 mm by modifying the side baffles. The number of particles is set to 10,000, and the contents of the eight particle sizes follow a uniform distribution. The density of the screen panel is set as 1.35×10^{-6} kg/mm³. Two parameters in the strain-energy density function are: C_{01}= 0.7 MPa and C_{10}= 2.8 MPa. The screen panel mesh is divided using hexahedra. The friction coefficients selected for the contacts between mineral particles and particles, between particles and the screen panel, and between particles and the baffle are 0.45, 0.48, and 0.63 respectively. The angular frequency ω is set as 68 rad · s^{-1} (Gong et al., 2020).

4. Results of simulation

4.1. The kinematic characteristics of particles and the screen panel

To investigate the kinematic characteristics of minerals on the screen panel of conventional constant-amplitude VFFS under different amplitude conditions, and the effects of different amplitudes on the motion characteristics of minerals on the screen panel of the variable-amplitude VFFS. Considering that when the relative amplitude of the MSF and FSF is excessively small, issues such as severe minerals accumulation and excessively long overall screening time are prone to occur, and when the relative amplitude is excessively large, severe deformation of the screen panel is likely to occur, and the screen panel is prone to damage. Therefore, the relative amplitudes of the MSF and FSF for the constant-amplitude VFFS were set as 4 mm, 6 mm, and 8 mm, respectively (as shown in Figs. 5(a), (b), and (c)), while the relative amplitudes of the MSF and FSF for the three screening zones of the variable-amplitude VFFS were set to 8 mm for screening zone I, 6 mm for screening zone II, and 4 mm for screening zone III (as shown in Fig. 5(d)). Both the constant-amplitude and variable-amplitude VFFS were configured with a screen panel inclination angle of 10° and an angular frequency of 68 rad ·s^{-1}. Simulation analysis was conducted on the motion states of minerals at the "inlet end" and "outlet end" after minerals loading (6.150 s), with the results presented in Fig. 5.

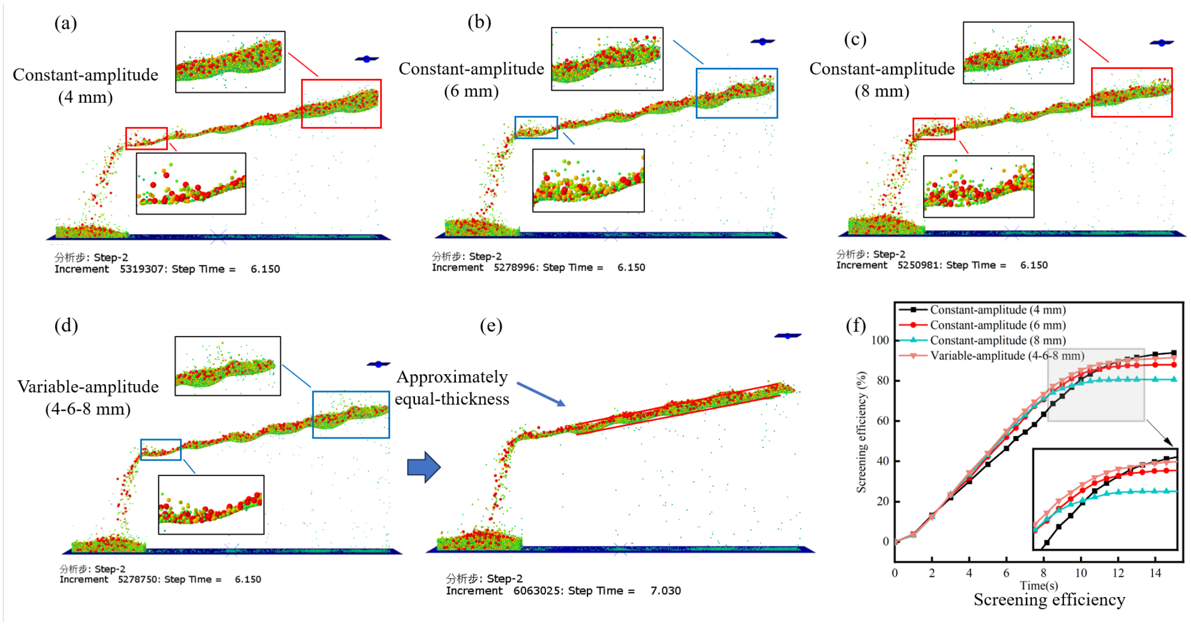

Fig. 5. Motion state of minerals at the "inlet end" and "outlet end" for the screening process under different conditions: (a) constant-amplitude (4 mm), (b) constant-amplitude (6 mm), (c) constant-amplitude (8 mm), (d) variable-amplitude (4-6-8 mm), (e) the variation-amplitude achieves approximate equal-thickness, (f)screening efficiency

As can be observed from Figs. 5(a), 5(b), and 5(c), during the constant-amplitude screening process of minerals, the accumulation of minerals at the "inlet end" gradually decreased with increasing relative amplitude of the MSF and FSF. Specifically, when the amplitude was 4 mm, pronounced mineral accumulation was observed, primarily attributed to the relatively small screen amplitude resulting in insufficient projection intensity for particles, preventing rapid backward conveyance after particle-screen contact and exacerbating mineral accumulation. With increasing amplitude to 8 mm, particles experienced stronger projection forces upon screen contact, effectively alleviating mineral accumulation at the "inlet end". As shown in Fig. 5(d), during the variable-amplitude screening of minerals, in screening zone I, the accumulation thickness of minerals at the "inlet end" was less than that of the constant-amplitude VFFS with an amplitude of 8 mm. In screening zone III, the mineral thickness at the "outlet end" exceeded that of the constant-amplitude relaxation screen with an amplitude of 4 mm. Therefore, when using a variable-amplitude VFFS to screen minerals, it is easier to make the minerals on the screen reach an approximately equal-thickness state, as shown in Fig. 5(e). As can be seen from Fig. 5(f), with the passage of time, the screening efficiencies of both variable-amplitude VFFS and constant-amplitude VFFS exhibit an upward trend. For the constant-amplitude VFFS with a relative amplitude of the MSF and FSF of 4 mm, although it has the highest final screening efficiency, its screening efficiency improves slowly in a short period, and the required screening time is long. For the constant-amplitude VFFS with a relative amplitude of the MSF and FSF of 8 mm, the time required to screen minerals is the shortest, but the final total screening efficiency is low. In contrast, the variable-amplitude VFFS shows a more remarkable increase in screening efficiency in the early stage compared with the other three, and its final screening efficiency is also relatively high. This indicates that when using a variable-amplitude VFFS for mineral screening, it can not only effectively mitigate mineral accumulation at the "inlet end" and alleviate related operational issues such as blockages and screening inefficiencies, but also improve mineral distribution across the screen panel to enable near-uniform thickness states and thereby enhance overall screening efficiency.

To further illustrate the differences in mineral distribution on the screen panel between constant-amplitude and variable-amplitude VFFS during the screening process, the displacement variations of the midpoint on the screen panel in the y-direction (the normal direction of the midpoint of the screen panel) over time after mineral loading completion were analysed. Considering the influence of mineral behaviour at the "inlet end" and "outlet end", the time-dependent y-direction displacements of four specific screen panels (2, 3, 4, and 5) were primarily evaluated, as shown in Fig. 6.

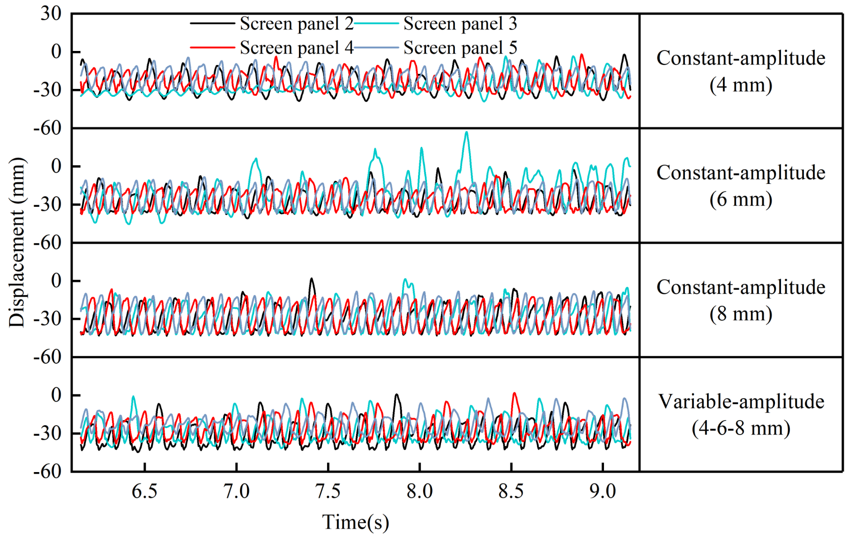

Fig. 6. The dynamic response of the midpoint of different screening panels in the y-direction

As indicated in Fig. 6, when the relative amplitude of the MSF and FSF for the constant-amplitude VFFS was 4 mm, insufficient screen amplitude prevented timely mineral conveyance downward, thereby causing accumulation on-screen panel 3 and resulting in smaller displacement fluctuations in the y-direction over time. Additionally, this operational state reflected that smaller amplitudes tend to prolong mineral residence time in each screening zone due to accumulation effects. When the relative amplitude of the MSF and FSF for the constant-amplitude VFFS was increased to 8 mm, the amplitude augmentation mitigated the direct mineral impact on the screen panel, leading to more regular time-dependent displacement variations in the y-direction at the screen midpoint. However, this operational adjustment concurrently caused a reduction in the contact time between screenable minerals and the screen apertures after particle-screen interaction, thereby resulting in decreased overall screening efficiency. For the variable-amplitude VFFS, the y-direction displacements of the midpoints of different screens remain complex and irregular over time.

On one hand, the screen is configured with a larger amplitude at the mineral "inlet end" to prevent accumulation and continuously reduces the amplitude to slow down the mineral flow, creating complex displacements for the midpoints of screen panels 2 and 3. In addition, when the materials on the screen transition from screen panel 2 to screen panel 3, the displacement of the midpoint of the screen panel will decrease accordingly due to the reduction in screen amplitude. However, after the materials pass through the screening zone Ⅰ, their quantity decreases, leading to an increase in the interaction between the screen panel and the materials. This results in complex variation states of the midpoints' displacement in the y-direction on both screen panel 2 and screen panel 3. On the other hand, reduced mineral quantity after screening in the front section and smaller amplitudes in the rear section enhance mineral impact on the screen, leading to complex displacements for the midpoints of screens 4 and 5. The continuously decreasing amplitude slows down mineral flow, thereby improving the screening efficiency of all screening zones in the variable-amplitude VFFS.

4.2. The influence of different factors on the variable amplitude screening process

As shown in Section 4.1, using a variable-amplitude VFFS during mineral screening is more beneficial for screening performance. Additionally, in the mineral screening process, besides the two critical parameters of angular frequency and relative amplitude of the MSF and FSF, the screen panel inclination angle is also a crucial influencing factor. Specifically, for the first group of variable-amplitude VFFS A, the relative amplitudes of the MSF and FSF in the screening zone are set as 7 mm in screening zone I, 5 mm in screening zone II, and 3 mm in screening zone III (variable amplitudes of 3-5-7 mm), For the second group of variable-amplitude VFFS B, the relative amplitudes of the MSF and FSF in the screening zone are 8 mm in screening zone I, 6 mm in screening zone II, and 4 mm in screening zone III (variable amplitudes of 4-6-8 mm). For the third group of variable-amplitude VFFS C, the relative amplitudes of the MSF and FSF in the screening zone are 9 mm in screening zone I, 7 mm in screening zone II, and 5 mm in screening zone III (variable amplitudes of 5-7-9 mm). Therefore, this paper investigates the effects of the relative amplitude of the MSF and FSF, angular frequency, and screen panel inclination angle on the screening performance of the variable amplitude VFFS.

4.2.1. Influence of angular frequency on screening performance

Considering the operational angular frequency of the VFFS (Gong et al., 2020), three angular frequencies of 68 rad · s^{-1}, 74 rad ·$s^{-1,}$ and 80 rad · s^{-1} are selected to investigate their effects on the screening performance of the three different variable-amplitude VFFS with the inclination angle being 10°, as shown in Fig. 7.

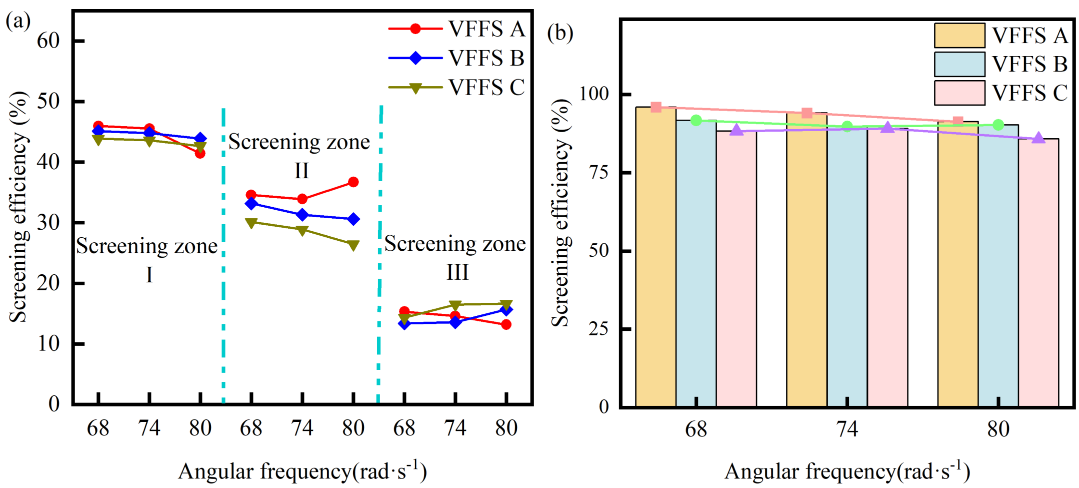

Fig. 7. The Influence of angular frequency on the screening efficiency of different VFFS:(a) different screening zones, (b) total screening efficiency

As shown in Fig. 7(a), in Screening Zone I, the screening efficiency of the variable-amplitude VFFS A, B, and C slightly decreased with increasing angular frequency, but the overall variation was relatively small. This is primarily due to mineral accumulation in screening zone I and the small screen panel inclination angle, which resulted in insignificant effects of angular frequency changes on screening efficiency in this zone. In Screening Zone II, the screening efficiency of variable-amplitude VFFS A significantly exceeded that of B and C. Notably, as the angular frequency increased, the efficiency of variable-amplitude A further improved, while B and C showed declines. This discrepancy arises from the relatively small relative amplitude of variable-amplitude A's MSF and FSF, which prevents excessive mineral projection and allows higher angular frequencies to enhance contact opportunities between screenable minerals and screen apertures. In Screening Zone III, the efficiency of variable-amplitude VFFS A decreased with increasing angular frequency, whereas the variable-amplitude B and C exhibited the opposite trend. On the one hand, after the materials of the variable-amplitude VFFS A pass through screening areas I and II, the number of screenable minerals is less than that of screens B and C. On the other hand, although the increase in angular frequency enhances the contact opportunities between minerals and the screen panel, the smaller amplitude of the variable-amplitude screen A results in a thicker material thickness in the screening area III. At this time, too high angular frequency will shorten the residence time of minerals, causing some minerals to fail to fully disperse and pass through the screen, thereby leading to a decrease in screening efficiency. Additionally, as shown in Fig. 7(b), under different variable-amplitude conditions, the total screening efficiency slightly decreased with increasing angular frequency. Nevertheless, all total screening efficiency values remained above 80%, indicating minimal overall variation. This observation demonstrates that changes in angular frequency exert some influence on the screening efficiency of each screening zone but have a relatively minor impact on the overall screening efficiency. However, during continuous machine operation, adjusting the angular frequency represents the most convenient method to alter mineral screening outcomes. Meanwhile, this finding underscores that angular frequency serves as a critical and non-negligible factor affecting the mineral screening process of variable-amplitude VFFS.

4.2.2. Influence of amplitude on screening performance

Considering that the variation of the relative amplitude of the MSF and FSF significantly affects the motion state of minerals at the "inlet end" and "outlet end" during the screening process of variable-amplitude VFFS, the influence of three groups of different amplitudes on the screening efficiency of variable-amplitude VFFS was investigated with the inclination angle of screen panel being 10°, as shown in Fig. 8.

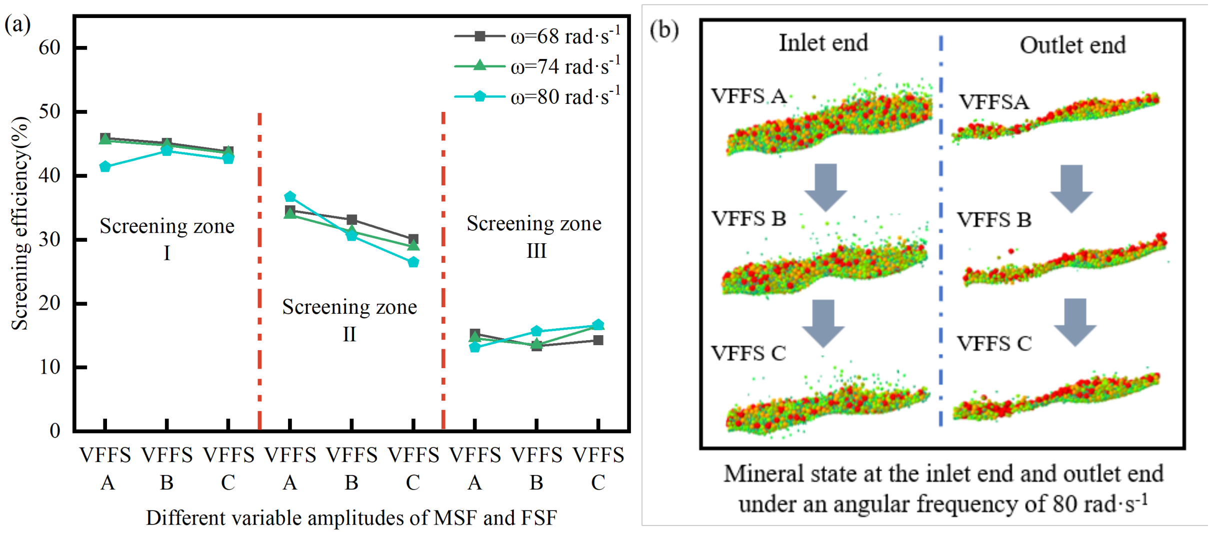

Fig. 8. Effects of amplitude on screening efficiency and material motion state in different variable-amplitude VFFS: (a) different screening zones, (b) motion state of minerals

From Fig. 8(a), it can be seen that when the angular frequency is kept constant, the screening efficiencies of different screening zones show different characteristics with the change of the relative amplitude of the MSF and FSF. In particular, in screening zone I, for the variable-amplitude VFFS with three different relative amplitudes of the main MSF and FSF, when the angular frequency is 80 rad·s^{-1}, the screening efficiency first increases with the increase of the amplitude and then gradually decreases. This is mainly because the high angular frequency of variable-amplitude C and the increased amplitude of the mineral at the "inlet end" promote the screening efficiency of the mineral in screening zone I. However, further increasing the amplitude shortens the mineral retention time, resulting in the screening efficiency generally being lower than that at other angular frequencies, as shown by the state of the mineral at the "inlet end" in Fig. 8(b). In screening zone II, the interval screening efficiencies of the variable-amplitude VFFS with three different relative amplitudes of the MSF and FSF all show a downward trend with the increase of the relative amplitude of the MSF and FSF. The decline is most obvious when the angular frequency is 80 rad·s^{-1}. In screening zone III, for the variable-amplitude VFFS with three different relative amplitudes of the MSF and FSF, when the angular frequencies are 68 rad·s^{-1} and 74 rad·s^{-1}, the screening efficiency first decreases and then increases with the increase of the amplitude. However, when the angular frequency is 80 rad·s^{-1}, it shows a continuous upward trend. This is mainly because the large amplitude at the "inlet end" promotes the dispersion of the mineral and the rapid backward flow of the mineral, but it may cause the screenable mineral not to be screened in time. The smaller amplitude at the "outlet end" prolongs the mineral residence time, allowing the unscreened mineral to be further screened, thus improving the screening efficiency, as shown by the state of the mineral at the "outlet end" in Fig. 8(b). Thus, reasonably adjusting the relative amplitude of the MSF and FSF has a more significant impact on the overall screening efficiency compared with the angular frequency.

4.2.3. Influence of screen panel inclination on screening performance

Given the significant impact of screen panel inclination angle on the screening efficiency of variable-amplitude VFFS, an analysis was conducted to investigate its effects on screening efficiency, the relative amplitude of the MSF and FSF, and angular frequency, as shown in Figs. 9 and 10.

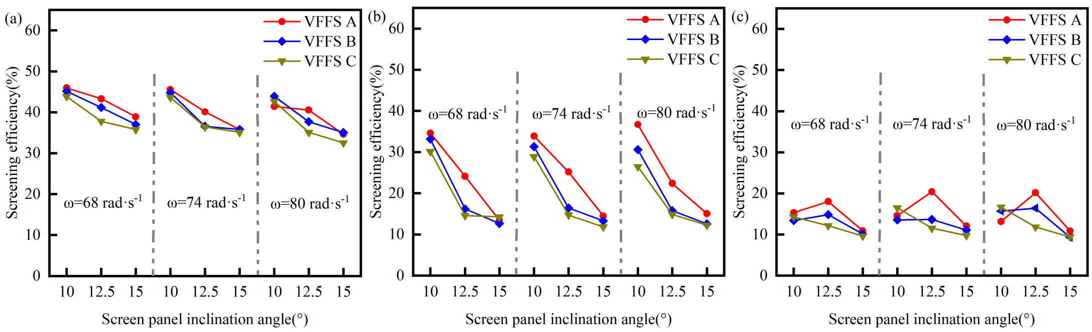

Fig. 9. Effects of inclination angle on the screening efficiency of Variable-Amplitude VFFS at different amplitudes: (a) screening zone I (b) screening zone II (c) screening zone III

As shown in Figs. 9(a), 9(b), and 9(c), variable-amplitude VFFS with three different relative amplitudes of the MSF and FSF exhibit distinct characteristics in screening efficiency across different screening zones as the screen panel inclination angle changes. Specifically, in screening zone I, the screening efficiency differences among variable-amplitude VFFS with different relative amplitudes of the MSF and FSF are minimal. This indicates that the screening efficiency in this zone is less affected by variations in the screen panel inclination angle, and the differences between different relative amplitudes of the MSF and FSF are not significant. In screening zone II, the screening efficiency of all three groups of variable-amplitude VFFS with different relative amplitudes of the MSF and FSF sharply decreases as the screen panel inclination angle increases, dropping from above 30% to approximately 15%. The decline amplitude significantly exceeds that in screening zone I, and notable differences in screening efficiency exist among different amplitudes within this zone, demonstrating that changes in the screen panel inclination angle have a more pronounced impact on screening efficiency in screening zone II. In screening zone III, the screening efficiencies of the three groups of variable-amplitude VFFS with different relative amplitudes of the MSF and FSF intersect, reflecting the combined influence of screen panel inclination angle and relative amplitude of the MSF and FSF on screening efficiency in this zone.

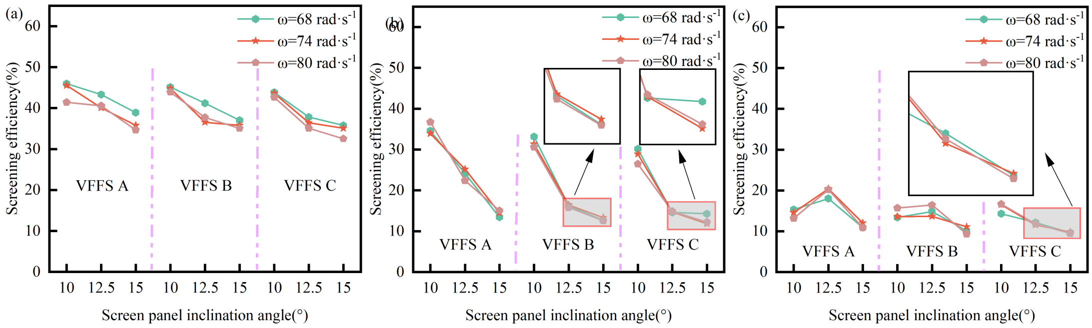

Fig. 10. Effects of inclination angle on the screening efficiency of variable-amplitude VFFS at different angular frequencies: (a) screening zone I (b) screening zone II (c) screening zone III

As shown in Figs. 10(a), 10(b), and 10(c), when the angular frequency of variable-amplitude VFFS with three groups of different relative amplitudes of the MSF and FSF increased from 68 rad $\cdot$ s^{-1} to 80 rad $\cdot$ s^{-1}, the screening efficiency in each screening zone exhibited distinct responses to variations in the screen panel inclination angle. As an illustration, in screening zone I, the screening efficiency decreased with increasing screen panel inclination angle. Moreover, the efficiencies corresponding to different angular frequencies were comparable, indicating that angular frequency in this zone was minimally influenced by the screen panel inclination angle. In screening zone II, the screening efficiency dropped to less than 15% as the screen panel inclination angle increased, with a decline rate significantly greater than that in screening zone I. Substantial differences in screening efficiency were also observed across different angular frequencies, suggesting that both angular frequency and the relative amplitude of the MSF and FSF in this zone were strongly affected by the screen panel inclination angle. In screening zone III, the screening efficiency demonstrated divergent trends with increasing angular frequency, indicating that within specific inclination angles, certain angular frequency ranges can enhance screening efficiency.

5. Multi-parameter response surface optimization

5.1. Experimental design

When exploring the influencing factors that the variable-amplitude VFFS is subjected to during the process of screening minerals, the above-mentioned study mainly determines the influence of each factor on the mineral's screening effect through single-factor experiments. However, this approach has limitations, as it cannot fully reveal the interactions between factors or the degree of influence of each factor. Additionally, due to the inability of Design-expert software to directly display the relative amplitude values of the MSF and FSF across the three screening zones of variable-amplitude VFFS, the median values of the relative amplitudes of the MSF and FSF in the three screening zones were selected as representatives. Therefore, this study utilized the Box-Behnken design method in the software to design response surface methodology (RSM) experiments with 3 factors and 3 levels. The design factors and levels of the multi-factor RSM experiments, along with relevant parameters, are presented in Table 2.

This study aims to explore the variation characteristics of the total screening efficiency of minerals and screening time under different combinations of factors. According to the set experimental factors and levels, 17 sets of combination schemes are obtained, as shown in Table 3.

A polynomial was employed to construct the approximate functional relationship between the objective function and influencing factors. Analysis of variance (ANOVA) was performed on the measured data to evaluate the accuracy of the response surface model. The response surface fitting parameters are presented in Tables 4 and 5. For variable-amplitude VFFS. Therefore, the quadratic regression equations relating the screen panel inclination angle, angular frequency, and relative amplitude of the MSF and FSF to the total screening efficiency (Y_1) and total screening time (Y_2) are as follows:

$$\begin{cases} Y_1 = 66.68 - 6.61X_1 - 16.16X_2 - 1.19X_3 - 0.17X_1X_2 - 0.11X_1X_3 - 0.35X_2X_3 \\ \quad + 3.96X_1^2 + 4.88X_2^2 + 3.11X_3^2 \\ Y_2 = 9.40 - 2.06X_1 - 4.97X_2 - 0.1375X_3 - 1.77X_1X_2 - 0.0875X_1X_3 - 0.3575X_2X_3 \\ \quad + 1.55X_1^2 + 3.12X_2^2 + 0.8213X_3^2 \end{cases} \tag{10}$$

Table 2. Factors and levels of the multifactor RSM test

Level	Factors		
	Relative amplitudes of the MSF and FSF (mm)	Screen panel inclination angle (°)	Angular frequency (rad.s^{-1})
-1	3-5-7	10	68
0	4-6-8	12.5	74
1	5-7-9	15	80

Table 3. Table caption experimental design schemes and results of the RSM

Experiment number	Relative amplitudes of the MSF and FSF (X_1/ mm)	Screen panel inclination angle (X_2/ °)	Angular frequency (X_3/ rad s^{-1})	Total screening efficiency (Y_1/ %)	Total screening time (Y_2/ s)
1	0	0	0	66.68	9.40
2	0	-1	1	90.20	17.16
3	1	-1	0	89.08	16.00
4	0	1	1	56.92	8.90
5	-1	0	1	83.16	14.25
6	1	1	0	56.68	8.62
7	-1	1	0	62.32	8.60
8	0	-1	-1	91.72	18.50
9	0	0	0	66.68	9.40
10	-1	0	-1	85.48	14.00
11	0	1	-1	59.84	8.81
12	1	0	-1	64.56	9.46
13	0	0	0	66.68	9.40
14	0	0	0	66.68	9.40
15	-1	-1	0	94.04	23.05
16	1	0	1	61.80	9.36
17	0	0	0	66.68	9.40

5.2.Result analysis and simulation experimental validation

Analysis of variance was conducted on the regression model, and the results are shown in Tables 4 and 5. The regression model for Y_1 is significant (P<0.0006), with a determination coefficient R_1^2 of 0.9552 and an adjusted determination coefficient R_{adj1}^2 of 0.8977. The regression model for Y_2 is also significant (P<0.0001), with a determination coefficient R_2^2 of 0.9907 and an adjusted determination coefficient R_{adj2}^2 of 0.9787. It indicates that both the goodness of fit and the credibility of the regression equation are relatively high, the lack-of-fit test is not significant, and the experimental error is small. Therefore, this model can be used to predict the total screening efficiency.

It can be seen from Table 3 that the change in the screen panel inclination angle has a direct impact on the screening time. When the screen panel inclination angle of the variable-amplitude VFFS is relatively large, the total screening efficiency of the minerals is relatively low, but the screening time is

Table 4. Analysis of variance of total screening efficiency

Source	Sum of Squares	df	Mean Square	F-value	P-value	Significance
Model	2681.22	9	297.91	16.60	0.0006	Significant
A-X_1	349.54	1	349.54	19.47	0.0031	
B-X_2	2089.16	1	2089.16	116.40	< 0.0001	
C-X_3	11.33	1	11.33	0.6312	0.453	
AB	0.1156	1	0.1156	0.0064	0.9383	
AC	0.0484	1	0.0484	0.0027	0.96	
BC	0.49	1	0.49	0.0273	0.8734	
A^2	66.19	1	66.19	3.69	0.0963	
B^2	100.48	1	100.48	5.60	0.0499	
C^2	40.59	1	40.59	2.26	0.1763	
Residual	125.64	7	17.95			
Lack of Fit	125.64	3	41.88			
Pure Error	0	4	0			
Cor Total	2806.85	16				

Table 5. Analysis of variance of total screening time

Source	Sum of Squares	df	Mean Square	F-value	P-value	Significance
Model	303.18	9	33.69	82.83	< 0.0001	Significant
A-X_1	33.87	1	33.87	83.27	< 0.0001	
B-X_2	197.81	1	197.81	486.39	< 0.0001	
C-X_3	0.1513	1	0.1513	0.3719	0.5612	
AB	12.50	1	12.5	30.73	0.0009	
AC	0.0306	1	0.0306	0.0753	0.7917	
BC	0.5112	1	0.5112	1.26	0.2992	
A^2	10.07	1	10.07	24.75	0.0016	
B^2	41.02	1	41.02	100.86	< 0.0001	
C^2	2.84	1	2.84	6.98	0.0333	
Residual	2.85	7	0.4067			
Lack of Fit	2.85	3	0.9489			
Pure Error	0	4	0			
Cor Total	306.03	16				

short and the processing capacity is high. Conversely, if the screen panel inclination angle is relatively small, the total screening efficiency of the materials is relatively high, but it will lead to a decrease in the processing capacity of the variable-amplitude VFFS for the minerals and a longer screening time. Therefore, during the optimization process, considering the screening efficiency and time, by combining the results of the analysis of variance with the Design-Expert 13 software, the response optimizer is employed to optimize and analyze the combination of horizontal factors that influence the total screening efficiency and time. The results are illustrated in Figs. 11 and 12. According to the actual production and process adjustment parameters, the finally determined optimal parameter combination is as follows: when the relative amplitudes of the MSF and FSF in the three screening zones are 8 mm in screening zone I, 6 mm in screening zone II, and 4 mm in screening zone III, respectively, screen panel inclination angle at 11°, and angular frequency at 76 rad$\cdot$s^{-1}, the variable amplitude VFFS has a higher screening efficiency (84.96%) and a shorter screening time (14.51 s). When compared with the optimization results, the relative errors are 8.33% and 8.48% respectively. It can be seen that the optimization results have a relatively high degree of credibility.

6. Conclusions

In this paper, by applying the theory of multi-mass dynamics to the establishment of a dynamic model of the multi-mass VFFS, the amplitude regulation in different regions of the investigated VFFS was

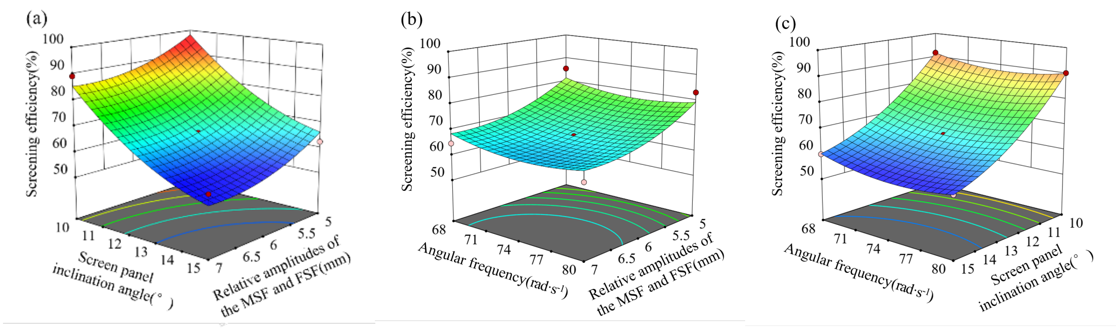

Fig. 11. Response surface of the total screening efficiency

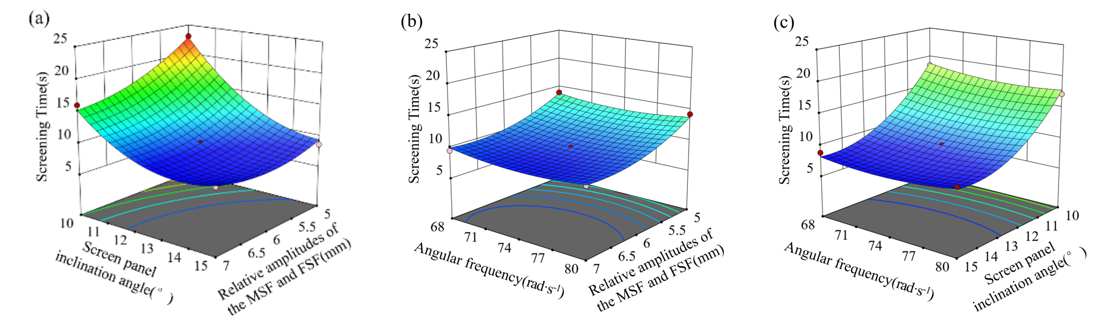

Fig. 12. Response surface of the total screening time

achieved by adjusting its dynamic parameters, and the relative amplitude between the MSF and FSF can reach a predefined target value using the optimization algorithm, revealing the regulation mechanism of the multi-mass VFFS.

Then, combining the advantages of the FEM and DEM, a coupling simulation model of multiple flip-flow screen panels and minerals was established, and the influence of various dynamic parameters on the screening efficiency of the variable-amplitude VFFS was revealed: an increase in angular frequency can enhance the screening efficiency, yet the efficiency will decline if it is excessively. Adjusting the relative amplitude in different screening regions can optimize the mineral distribution and improve the screening efficiency. Increasing the inclination angle of the screening panel can increase the processing capacity, but excessive inclination leads to a sharp decline in screening efficiency.

Finally, employing a three-factor and three-level orthogonal experimental design in tandem with response surface optimization to evaluate the effect of screen panel inclination, angular frequency, and relative amplitudes on the screening performance and time. Results revealed that the optimal balance between screening efficiency and screening time can be realized when the relative amplitude of the three regions of variable-amplitude VFFS are 4 mm, 6 mm, and 8 mm, respectively, with a screen inclination of 11° and an angular frequency of 76 rad · s^{-1}.

This research achievement not only enriches the vibration theory of multi-mass systems and mineral screening theory but also helps improve the processing capacity and screening efficiency of screening equipment. Particularly in the screening of wet fine-grained minerals, it can alleviate the problem of screen clogging and optimize production efficiency. Additionally, it provides a theoretical basis for the selection of screening equipment required for different minerals.

Acknowledgments

The research is financially supported by the National Natural Science Foundation of China (52204267), the Key Scientific and Technological Project of Henan Province (252102221006, 242102220007, 252102221005), and the Discipline Innovation and Intelligence Introduction Program of Higher Education Institutions (25A460013).

References

AXBARI, H., ACKAH, L., MOHANTY, M., 2017. *Performance optimization of a new air table and flip-flow screen for fine particle dry separation.* International Journal of Coal Preparation and Utilization, 40(9):581-603.

DUAN, C., YUAN, J., PAN, M., HUANG, T., JIANG, H., ZHAO, Y., QIAO, J., WANG, W., YU, S., LU, J., 2021. *Variable elliptical vibrating screen: Particles kinematics and industrial application.* International Journal of Mining Science and Technology, 31:1013-1022.

DONG, K., YU, A., BRAKE, I., 2009. *DEM simulation of particle flow on a multi-deck banana screen.* Minerals Engineering, 22:910-920.

FERNANDEZ, J., CLERY, P., SINNOTT, M., MORRISON, R., 2011. *Using SPH one-way coupled to DEM to model wet industrial banana screens.* Minerals Engineering, 24:741-753.

GONG, S., WANG, X., OBERST, S., 2018. *Non-linear analysis of vibrating flip-flow screens.* MATEC Web of Conferences, 221, 04007.

GONG, S., WANG, X., YU, C., ZHAO, G., LIN, D., XU, N., ZHU, G., 2019. *Dynamic analysis of vibrating flip-flow screen based on a nonlinear model of shear spring*. Journal of China Coal Society, 44(10):3241-3249.

GONG, S., OBERST, S., WANG, X., 2020. A*n experimentally validated rubber shear spring model for vibrating flip-flow screens*. Mechanical Systems and Signal Processing, 139, 106619.

GUO, J., GONG, S., QIAO, Z., WANG, C., WU, T., GAO, Y., 2024. *Study on dynamic characterization of four-mass flip-flow screen.* Coal Engineering, 56(11):195-201.

HOU, X., WANG, W., PAN, J., MAO, P., ZHANG, S., DUAN, C., 2024. *Optimization of flip-flow screen plate based on DEM-FEM coupling model and screening performance of fine minerals.* Minerals Engineering, 211, 108694.

HUANG, L., LIU, Y., LU J., YU, S., MIAO, P., WU, J., QIAO, J., JIANG, H., 2022. *Research of the collision mechanics model and time-frequency characteristics during the multistage variable-inclination screening process for clean coal*. ACS OMEGA, 7(16):13963-13975.

JIANG, H., ZHAO, Y., DUAN, C., ZHANG, C., DIAO, H., WANG, Z., FAN, X., 2017. *Properties of technological factors on screening performance of coal in an equal-thickness screen with variable amplitude.* Fuel, 188:511–521.

JIANG, H., LIU Y., Li W., WEN, P., HUANG, L., YUAN, J., YU, S., PAN, M., DUAN, C., 2024. *Parameter optimization and spatio-temporal distribution of material for variable trajectory combined equal-thickness screen.* Powder Technology, 438, 119590.

LI, Z., XU, Y., JIA, P., SI, Q., TONG, X., 2021. *Study on screening performance and parameters optimization of double relatively independent vibrating screen.* Physicochemical Problems of Mineral Processing, 57(6):160-172.

LIN, D., XU, N., YU, C., GENG, R., WANG, X., GONG, S., 2022. *Nonlinear model of vibrating flip-flow screens that considers the effects of screen panels.* IEEE ACCESS, 3161966.

LIN, D., JI, J., WANG, X., WANG, Y., XU, N., NI, Q., ZHAO, G., FENG, K., 2023. *A rigid-flexible coupled dynamic model of a flip-flow vibrating screen considering the effects of processed materials*. Powder Technology, 427, 118753.

LIN, D., JI, J., YU, C., WANG, C., WANG, X., XU, N., 2023. *A non-linear model of screen panel for dynamics analysis of a flip-flow vibrating screen.* Powder Technology, 418, 118312.

QIAO, J., DUAN C., JIANG, H., ZHAO, Y., CHEN, J., HUANG, L., WEN, P., WU, J., 2018. *Research on screening mechanism and parameters optimization of equal thickness screen with variable amplitude based on DEM simulation.* Powder Technology, 331:296-309.

SHI, W., WANG, W., MAO, P., HOU, X., ZHANG, S., DUAN, C., 2025. *Research on the dry deep flip-flow screening of ilmenite and its pre-throwing tail processing technology*. Minerals, 15, 308.

XIONG, X., NIU, L., GU, C., WANG, Y., 2017. *Vibration characteristics of an inclined flip-flow screen panel in banana flip-flow screens.* Journal of Sound and Vibration, 411:108-128.

XU, N., WANG, X., LIN, D., ZUO, W., 2024. *Numerical simulation and optimization of screening process for vibrating flip-flow screen based on discrete element method–finite element method–multi-body dynamics coupling method*. Minerals, 14, 278.

WANG, C., LIU, Q., YANG, L., 2024. *The MFBD-DEM coupling simulation approach for the investigation of granules screening efficiency in 4-DOF flip-flow screen.* Granular Matte, 26:5.

WU, B., ZHANG, X., NIU, L., XIONG, X., DONG, Z., TANG, J., 2019. *Research on sieving performance of flip-flow screen using two-way particles-screen panels coupling strategy.* IEEE ACCESS, 2938847.

WU, J., LIU, C., JIANG, H., 2020. *A vibration-test-based calculation method of screening material mass of a mining crank-link type flip-flow screen.* Energy Sources Part A Recovery Utilization and Environmental Effects, 1778139: 1-21.

WU, B., CAO, S., LUO, Q., 2025. *Dynamic characteristics of vibrating flip-flow screens considering material impact force*. International Journal of Mechanical System Dynamics, 1-17.

YU, C., WANG, X., GONG, S., PANG, K., ZHAO, G., ZHOU, Q., LIN, D., XU, N., 2021. *Stability analysis of the screening process of a vibrating flip-flow screen*. Minerals Engineering, 163, 106794.

ZHANG, X., WU, B., NIU, L., XIONG, X., DONG, Z., 2019. *Dynamic characteristics of two-way coupling between flip-flow screen and particles based on DEM*. Journal of China Coal Society, 44(6):1930-1940.

ZHAO, L., LIU, C., YAN, J., JIANG, X., ZHANG, Y., 2010. *Numerical simulation of particles flow on the vibrating screen plate using a 3D discrete element method.* Journal of China University of Mining & Technology, 39(3):414-419.

ZHAO, G., PU, K., XU, N., GONG, S., WANG, X., 2023. *Simulation of particles motion on a double vibrating flip-flow screen surface based on FEM and DEM coupling*. Powder Technology, 421, 118422.

ZHENG, Q., XU, M., CHU, K., PAN, R., YU, A., 2016. *A coupled FEM/DEM model for pipe conveyor systems: Analysis of the contact forces on belt*. Powder Technology, 314:480-489.